Research Article

Rosa hybrida Petal Extract Exhibits Antitumor Effects by Abrogating Tumor Progression and Angiogenesis in Bladder Cancer Both In Vivo and In Vitro

Byungdoo Hwang[1], Yujeong Gho[1], Hoon Kim[1], Sanghyun Lee[2], Soon Auck Hong[3], Tae Jin Lee[3], Soon Chul Myung[4], Seok-Joong Yun[5], Yung Hyun Choi[6], Wun-Jae Kim[5], and Sung-Kwon Moon[1] (iD)

Abstract
The edible *Rosa hybrida* (RH) petal is utilized in functional foods and cosmetics. Although the biological function of RH petal extract is known, mechanism of action studies involving tumor-associated angiogenesis have not yet been reported. Herein, we investigated the regulatory effect of the ethanol extract of RH petal (EERH) on tumor growth and tumor angiogenesis against bladder cancer. EERH treatment inhibited the bladder carcinoma T24 cell and 5637 cell proliferation because of G_1-phase cell cycle arrest by inducing p21WAF1 expression and reducing cyclins/CDKs level. EERH regulated signaling pathways differently in both cells. EERH-stimulated suppression of T24 and 5637 cell migration and invasion was associated with the decline in transcription factor-mediated MMP-9 expression. EERH oral administration to xenograft mice reduced tumor growth. Furthermore, no obvious toxicity was observed in acute toxicity test. Decreased CD31 levels in EERH-treated tumor tissues led to examine the angiogenic response. EERH alleviated VEGF-stimulated tube formation and proliferation by downregulating the VEGFR2/eNOS/AKT/ERK1/2 cascade in HUVECs. EERH impeded migration and invasion of VEGF-induced HUVECs, which is attributed to the repressed MMP-2 expression. Suppression of neo-microvessel sprouting, induced by VEGF, was verified by treatment with EERH using the ex vivo aortic ring assay. Finally, kaempferol was identified as the main active compound of EERH. The present study demonstrated that EERH may aid the development of antitumor agents against bladder cancer.

Keywords
ethanol extract of *Rosa hybrida*, bladder cancer, tumor angiogenesis, bladder cancer cells, kaempferol, xenograft mice

Submitted December 20, 2021; revised May 11, 2022; accepted June 30, 2022

Introduction

Bladder cancer is the 10th most common cancer, known for its increased incidence, high recurrence risk, and fatal mortality rates.[1] In 2018, approximately 550 000 new cases were diagnosed, and 200 000 deaths were recorded worldwide.[1] Bladder cancer can be classified as either a non-muscle-invasive bladder cancer (NMIBC) or muscle-invasive bladder cancer (MIBC).[2] The majority of patients demonstrate NMIBC, whereas 25% of the patients demonstrate MIBC.[3] Upon transurethral resection of bladder tumors, NMIBC exhibits high recurrence and can even advance to MIBC, which is associated with increased lethal mortality.[3] Although considerable efforts are being made to develop novel agents or chemical compounds for the treatment of patients with MIBC, effective and safe therapeutic options

[1]Department of Food and Nutrition, Chung-Ang University, Anseong, South Korea
[2]Dpartment of Plant Science and Technology, Chung-Ang University, Anseong, South Korea
[3]Department of Pathology, College of Medicine, Chung-Ang University, Seoul, South Korea
[4]Department of Urology, College of Medicine, Chung-Ang University, Seoul, South Korea
[5]Department of Urology, Chungbuk National University, Cheongju, Chungbuk, South Korea
[6]Department of Biochemistry, College of Oriental Medicine, Dong-Eui University, Busan, South Korea

Corresponding Author:
Sung-Kwon Moon, Department of Food and Nutrition, Chung-Ang University, 4726 Seodong-Daero, Daedeok-Myeon, Anseong, 17546, Republic of Korea.
Email: sumoon66@cau.ac.kr

are very limited.[4] Hence, it is necessary to develop effective novel antitumor agents against MIBC.

Common patterns of MIBC involve the proliferation, migration, and invasion of bladder cancer cells.[5-7] During neoplastic propagation, cancer cells tend to proliferate and metastasize via the multiple steps of biological processes, including the control of signaling pathways and cell cycle.[5-7] Uncontrolled tumor cell proliferation is involved in the phosphorylation of mitogen-activated protein kinases (MAPKs) and phosphoinositide 3-kinase/serine-threonine kinase (PI3K/AKT) signaling.[6-9] In addition, advanced type of tumor cells are significantly associated with dysregulated cell cycle control because of the changes in cell cycle regulators, such as cyclins, cyclin-dependent kinases (CDKs), and CDK inhibitors (CKIs), during the G_1- to S-phase transition.[6-8,10] Matrix metalloproteinases (MMPs), especially MMP-9, participate in migration and invasion of cancer cells during the advanced stage of bladder cancer.[11-14] Several transcription factors, such as the nuclear factor-kappa-B (NF-κB), Sp-1, and AP-1, were observed to enhance the expression levels of MMP-9 in bladder cancer cells.[6,7,15,16]

Angiogenesis is the intricate pathological process involved in the formation of neovessels from the pre-existing ones, and it is regarded as one of the main hallmarks of progression and development of tumor cells.[17,18] Moreover, angiogenesis is tightly controlled by multiple series of interactive processes, such as endothelial cells (ECs), degradation of the extracellular matrix, and angiogenic factors.[18,19] Proliferation and migration of ECs to establish new vessels is an essential process during tumor angiogenesis.[20] Vascular endothelial growth factor (VEGF) is one of the most potent angiogenic activators that stimulates proliferation and migration of ECs as well as formation of neovessels by binding with its receptor, vascular endothelial growth factor receptor-2 (VEGFR-2).[21-24] Binding of VEGF to VEGFR-2 activates the downstream signaling molecules, such as the extracellular signal-regulated kinase (ERK)-1/2 and AKT, which activate endothelial nitric oxide synthase (eNOS) expression in ECs.[25-27] VEGF-mediated activation promotes degradation of the extracellular matrix by MMPs, leading to migration of cells and formation of new vessels.[28,29]

Although the development of anticancer drugs for bladder cancer treatment has been studied for decades, therapies have drug resistance and serious side effects.[30] Thus, the development of edible natural origin sources as alternative or complementary therapies with fewer side effects is urgent. Previous reports have shown that curcumin derived from *Curcuma longa* inhibits the progression of bladder cancer through cell cycle arrest, anti-angiogenesis, apoptosis as well as growth inhibition.[31-33] In addition, several in vitro and in vivo studies reported that resveratrol, a natural flavonoid compound occurring in peanuts, berries, and grapes, has antitumor effects on bladder cancer including cell cycle arrest, apoptosis, and inhibition of cell mobility.[34,35] Various natural origin extracts and their compounds have been suggested

the anticancer potential against bladder cancer treatment.[36] However, the inhibitory effects of *Rosa hybrida* (RH) in bladder cancer have not yet been fully understood.

The edible petals of RH are widely used as a reliable source of functional human nutrients as well as aromatic oils in the cosmetic industry.[37] In addition, RH petals contain numerous biological compounds, including gallic acid, kaempferol, and other volatile compounds, exhibiting antidiabetic, anti-inflammatory, anti-allergic, anti-atherogenic, and neuroprotective effects.[38-42] It has been revealed that RH petals may suppress the proliferation of several cancer cell lines in vitro.[43,44] However, the potential molecular mechanisms of antitumor effects by RH petals in vitro and in vivo have not been reported. Therefore, we investigated the precise action mechanisms of antitumor effects and angiogenesis inhibition effects of the RH extracts in bladder cancer using both in vitro experiments and in vivo mouse model. In addition, safety test was performed by using the oral acute toxicity model. The active compound of RH petals against antitumor effects was analyzed.

Materials and Methods

Materials

Antibodies against phospho-p38MAPK (#9211), phospho-ERK1/2 (#9101), phospho-c-Jun NH2-terminal kinase (JNK; #9251), phospho-AKT (#9271), p38MAPK (#9212), ERK1/2 (#9102), JNK (#9258), AKT (#9272), Mouse IgG Isotype Control (#5415S), and Normal rabbit IgG (#2729S) were purchased from Cell Signaling (Danvers, MA, USA). Antibodies against cyclin E (sc-247), cyclin D1 (sc-8396), cyclin-dependent kinase (CDK)-4 (sc-23896), CDK2 (sc-6248), p27KIP1 (sc-1641), p53 (sc-126), glyceraldehyde 3-phosphate dehydrogenase (GAPDH, sc-47724), and p21WAF1 (sc-6246) were obtained from Santa Cruz Biotechnology Inc. (Santa Cruz, CA, USA). Antibodies against VEGFR-2 (#2479), eNOS (#2479), phospho-VEGFR-2 (#4991), and phospho-eNOS (S1177) were purchased from Cell Signaling. Antibodies against MMP-2 (#AB19167) and MMP-9 (#04-1150) were obtained from Millipore (Massachusetts, USA). Human recombinant VEGF (293-VE) was purchased from R&D Systems (Minneapolis, USA). LY294002, SB203580, SP600125, and U0126 were obtained from Calbiochem (San Diego, CA, USA). The nuclear extraction kit and *electrophoretic mobility shift assay* (EMSA) kit (AY1XXX) were purchased from Panomics (Fremont, USA). Antibody against CD31 was obtained from BD PharMingen (San Diego, CA, USA).

Preparation of the ethanol extract of R. hybrid petal (EERH) and isolation of kaempferol

R. hybrida was obtained from Jincheon Agricultural Technology Center (Chungbuk, Korea). The compounds in

dried petals (1.96 kg) were extracted with ethanol at 80°C for 3 hours. The extract was filtered and concentrated under reduced pressure. The concentrated ethanol extract (62.39 g) was subsequently partitioned with different solvents, including *n*-hexane (3.80 g), CHCl$_3$ (1.50 g), EtOAc (9.60 g), and *n*-BuOH (6.70 g). Sub-fractions (a-, b-, c-, and d-fractions) were combined by elution of gradient solvents with CHCl$_3$ and MeOH from the EtOAc fraction. A portion of the d-fraction was subjected to open column chromatography using silica gel as the stationary phase and a stepwise gradient of CHCl$_3$ and MeOH as the mobile phase. Then, kaempferol from subfraction 41 of the EtOAc fraction was collected and analyzed using ^{1}H- and ^{13}C-nuclear magnetic resonance and electron ionization mass spectrometry.

Cell culture

T24 (high-grade; grade-3) cell lines were purchased from the American Type Culture Collection (Manassas, VA, USA). T24 cells were cultured in the Dulbecco's modified Eagle's medium. The human bladder cancer 5637 (low-grade; grade-2) cell lines were obtained from Korea Cell Line Bank (Seoul, Korea). 5637 cells were grown in RPMI1640 (Sigma-Aldrich, San Diego, CA, USA). All the media were supplemented with 10% fetal bovine serum (FBS, 35-010-CV, Corning, NY, USA), 100 µg/mL streptomycin, and 100 U/mL penicillin at 37°C and 5% carbon dioxide (CO$_2$) in a humidified incubator. Primary human umbilical vascular endothelial cells (HUVECs) were obtained from Lonza (Walkersville, MD, USA). The cells were cultivated on 0.1% gelatin-coated plates (Sigma-Aldrich, San Diego, CA, USA) using an endothelial basic medium supplemented with EGM™-2 Bulletkit™ (Lonza) at 37°C and 5% CO$_2$ in a humidified incubator. All experiments of HUVECs were conducted during passages 2 and 5.

Cell viability (3-(4, 5-dimethylthiazol-2-yl)-2, 5-diphenyltetrazolium bromide (MTT) assay) and viable cell counting assay

The cells (6×10^3 cells/well) were cultured in 96-well plates. After the treatment of cells with EERH, the cells were incubated with the MTT solution (0.5 mg/mL, Sigma-Aldrich) for 1 hour. The solution was removed and dissolved in dimethyl sulfoxide (DMSO). The absorbances of samples were detected at 540 nm using a fluorescent plate reader. The viability of cells was quantified as a percentage relative to the untreated group (control). Cellular morphology was visualized under a phase-contrast microscope. For the cell counting assay, after the detachment of cells with a solution of 0.25% trypsin-0.2% ethylenediaminetetraacetic acid (EDTA) (Thermo Fisher Scientific, Waltham, MA, USA), the cells were combined with 0.4% trypan blue (Sigma-Aldrich), followed by gentle mixing. The stained cells were then loaded and counted using the chamber of a hemocytometer.

Cell cycle analysis

EERH-treated cells were trypsinized and fixed in 70% ethanol at −20°C for 24 hours. Then, the cells were washed with ice-cold phosphate-buffered saline (PBS), followed by incubation with the cell cycle assay buffer (1 mg/mL RNase A and 50 mg/mL propidium iodide). Distribution of the cell cycle phase was analyzed using a MUSE® Cell Analyzer installed with the analysis software (Merck Millipore, Germany).

Immunoblotting and immunoprecipitation

After washing with ice-cold PBS, the cells were resuspended in the lysis buffer (150 mM NaCl, 50 mM HEPES, pH 7.5, DTT, 2.5 mM, 1 mM EDTA, 2.5 mM, EGTA, 1 mM DTT, 0.1 mM, Na$_3$VO$_4$, 1 mM NaF, 10 mM β-glycerophosphate, 10% glycerol, 0.1 mM PMSF 0.1 mM, 0.1% Tween-20, 2 µg/mL aprotinin, and 10 µg/mL leupeptin) at 4°C for 30 minutes. Cells were scraped and maintained on ice for 10 minutes. After centrifugation of extracts at 12 000×*g* for 15 minutes at 4°C, the cell lysates were subjected to determine the total amount of protein using a BCA protein assay reagent kit (Thermo Fisher Scientific). Aliquots comprising 25 µg of total proteins were separated on 10% Sodium dodecyl sulfate-polyacrylamide gel electrophoresis (SDS-PAGE), and then transferred to nitrocellulose membranes (Hybond; GE Healthcare Bio-Sciences, Marlborough, MA, USA). The membranes were blocked in 5% skim milk for 2 hours, followed by incubation with primary antibodies and peroxidase-conjugated secondary antibodies. A chemiluminescence reagent kit (GE Healthcare Bio-Sciences, Marlborough, MA, USA) was employed to detect the immunocomplexes. For immunoprecipitation analysis, the cell lysates containing 200 µg proteins were reacted with the indicated antibodies at 4°C overnight, then followed by incubation with protein A-sepharose beads (sc2003, Santa Cruz) at 4°C for 2 hours. The immunoprecipitated complexes were collected, washed, and subjected to SDS-PAGE and immunoblotting. Each cell lysate was used as input and normal rabbit and mouse antibodies were used as IgG control.

Wound-healing migration assay

The cells (3×10^5 cells/well) were cultured in 6-well plates and pre-incubated with mitomycin C (5 µg/mL, #M4287, Sigma-Aldrich) to impede their proliferation for 2 hours. After the surface of the cells was scratched with crosses using a 2-mm-wide pipette tip, the culture plates were washed and fresh culture media containing the indicated

concentrations of EERH was added. The cells were further incubated for 24 hours, and then the EERH-treated cells migrating into the scraped area were photographed under an inverted microscope. The percentage of scratched area in each group was determined after treatment with EERH compared to the control group.

Invasion assay

The cells (2.5×10^4 cells/well) were cultivated in a serum-free culture medium containing indicated concentrations of EERH and mitomycin C ($5 \mu g/mL$) and incubated for 2 hours in the upper chamber of the transwell plates containing 8-μm pores (Sigma-Aldrich). Simultaneously, the culture medium supplemented with 10% FBS or VEGF was replenished and incubated in the lower chamber at 37°C for 24 hours. Cells that invaded the low chamber were fixed with ethanol and stained using 0.1% crystal violet in 20% ethanol. The stained cells in the lower plate were photographed and counted. The quantifications of invaded cells were expressed as a percentage of the control groups.

Zymography

MMP-9 activity was examined using gelatin zymographic assay.[6,7] Briefly, the cells were treated with various concentrations of EERH for 24 hours. Then, the conditioned medium was subjected to electrophoresis on a 0.25% gelatin-polyacrylamide gel. After washing the gel with 2.5% Triton X-100 solution for 15 minutes at room temperature, the gel was incubated with renaturing buffer (150 mM NaCl, 50 mM Tris-HCl, and 10 mM $CaCl_2$, pH 7.5) at 37°C overnight. Gel was stained and visualized using 0.2% Coomassie blue under a light box. Gelatinase MMP-9 activity was detected by visualizing a white band on a blue background.

EMSA

Nuclear proteins were extracted from EERH-treated cells using a nuclear extraction kit (AY2002, Panomics). Briefly, the EERH-treated cells were centrifuged, washed, followed by incubation in a buffer [10 mM KCl, 10 mM HEPES (pH 7.9), 1 mM DTT, 0.1 mM EGTA, 0.5 mM PMSF, and 0.1 mM EDTA] for 15 minutes on ice, and then, the cells were mixed with 0.5% of NP-40 rigorously. The nuclear pellet was obtained via centrifugation, and the nuclear extracts were prepared by extraction in a buffer compromising 400 mM NaCl, 20 mM HEPES (pH 7.9), 1 mM PMSF, 1 mM EGTA, 1 mM DTT, and 1 mM EDTA at 4°C for 15 minutes. Pre-incubation of the nuclear extract (10-20 μg) was performed at 4°C for 30 minutes using a 100-fold excessive amount of an unlabeled oligonucleotide encompassing the −79 position of the MMP-9 cis-acting element

of interest. The sequences designed in this study were: AP-1, CTGACCCCTGAGTCAGCACTT; Sp-1, GCCCAT TCCTTCCGCCCCCAGATGAAGCAG; and NF-κB, CAG TGGAATTCCCCAGCC. The solution mixture was then reacted with a buffer (25 mM HEPES buffer (pH 7.9), 0.5 mM EDTA, 0.5 mM DTT, 50 mM NaCl, and 2.5% glycerol) containing poly dI/dC ($2 \mu g$) and 5 fmol (2×10^4 cpm) of a Klenow end-labeled (^{32}P ATP) 30-mer oligonucleotide, which stretched the DNA-binding element of the MMP-9 promoter at 4°C for 20 minutes. The reaction solution was separated by using a 6% polyacrylamide gel electrophoresis system at 4°C. Upon the gel exposure to an X-ray film, the values of gray blots were visualized and analyzed using the ImagePro Plus 6.0 software (Media Cybernetics, Rockville, MD, USA).

Generation of the xenograft mice model

All animal experiments were approved by the Animal Care and Use Committee of Chung-Ang University (2017-00054). Male BALB/c nude mice (6-week-old, 22-26 g) were obtained from the Dae-Han Experimental Animal Center (Dea-Han Biolink Co., Chungbuk, Korea) and were maintained at Chung-Ang University Animal Care Facility. T24 cells (3.6×10^7) resuspended in 100 μL PBS containing 100 μL Matrigel matrix (BD Biosciences, NJ) were inoculated subcutaneously into the right back of each mouse. After tumor reached a volume size of approximately 200-400 mm³, these mice were randomly separated into 4 groups. Vehicle alone (5% v/v ethanol) and EERH (20 and 200 mg/kg) were administered orally every day for 20 days and cisplatin (5 mg/kg) was injected once in 2 days for 20 days. In mice fed with EERH, it was dissolved in absolute ethanol and diluted in water. Body weight, tumor volume, and general inspection were observed daily for 20 days. Tumor width (W) and length (L) were measured every 5 days by a Vernier caliper and calculated using the formula [Tumor volume = (W2 × L)/2]. After 20 days, the tumor volume reached approximately 1984 mm³. Then, the xenograft mice were sacrificed, dissected, and the tumor tissues were separated for measuring their weights. Tumors were investigated using hematoxylin and eosin (H&E) staining and CD31 immunohistochemistry staining. To count the number of cells, hematoxylin-stained nuclei from all stained slides were quantified using Image J 1.53r software (http://imagej.nih.gov/ij).

H&E staining and immunochemistry (CD31)

Tumor tissues or major organs were fixed with formalin, then subsequently embedded and blocked in paraffin. The 5-μm-thick formalin/paraffin sections were stained with 10% hematoxylin (Sigma-Aldrich) and 1% eosin (Sigma-Aldrich). For the CD31 staining, formalin-fixed,

paraffin-embedded sections obtained from tumor tissues were incubated with a PBS (pH 7.4) solution comprising 5% bovine serum albumin for 1 hour to block nonspecific proteins. Subsequently, the samples were incubated with CD31 primary antibody (1:100) at 4°C overnight. After washing in PBS, the sections were reacted with fluorescent secondary IgG antibody (1:300) at room temperature for 2 hours. The stained samples were photographed under a fluorescent microscope (Leica, Wetzlar, Germany).

Oral acute toxicity and biochemical parameters

Oral acute toxicity test was performed as per the Regulation of Good Laboratory Practice, which was inspected by the Ministry of Food and Drug Safety. BALB/c mice (6-week-old, female, 22-24 g) were obtained and randomized into 2 groups (control and 2000 mg/kg group). Mice were given 5% ethanol (control) or ERH (2000 mg/kg) once via oral gavage. During 14 days, bodyweight was recorded and clinical signs, including neurologic, behavioral, mortality, and any other abnormalities, were assessed daily between the 2 groups. After the experiment, all mice were sacrificed, and the major organs (liver, lung, and kidney) and blood were collected. The major organs were proceeded for H&E staining. For the biochemical analysis, blood samples taken from mice aorta were added to heparin-containing tubes. After centrifugation at 3000 rpm for 10 minutes, the level of plasma biochemical markers, such as creatinine, urea, alkaline phosphatase (ALP), alanine aminotransferase (ALT), and aspartate aminotransferase (AST), were evaluated using commercial kits (Abcam, Burlingame, CA, USA).

Colony tube formation assay

Colony tube formation assay for EERH was performed on the pre-coated Matrigel plates using VEGF-treated HUVECs.[7] Briefly, HUVECs containing various concentrations of EERH or 20 ng/mL of VEGF were cultured on the Matrigel-coated plates for 7 hours at 37°C. When network formation of the tube-like colony was established, their images were visualized using a phase-contrast microscope. The level of colony tube formation was determined by estimating the length of branched tubes.

Aortic ring assay ex vivo

Microvessel sprouting potential of VEGF was evaluated using the aortic ring ex vivo assay as described before[7] with simple modifications. The thoracic aortas obtained from the C57BL/6 mice were carefully cut into 1-1.5-mm-thick segments. The segments were embedded in each well of the Matrigel-coated plates, followed by incubation with growth medium incorporating EERH (20 and 40 μg/mL) and VEGF (50 ng/mL). During the 9-day incubation, outgrowth of microvessel sprouting from aorta was visualized using a phase-contrast microscope. The potential of endothelial tube sprouting was quantified by measuring the area of microvessel sprouting using the ImagePro Plus 6.0 software.

High-performance liquid chromatography-ultraviolet (HPLC–UV) analysis of kaempferol from EERH

Samples were prepared for HPLC analysis by dissolving 10 to 20 mg of the petal extracts in 1 mL MeOH. A standard stock solution was prepared by dissolving 1 mg kaempferol in 1 mL MeOH. All samples were filtered through a 0.45-μm polyvinylidene fluoride filter prior to use. An HPLC system was used, and chromatographic separation was achieved using an INNO C_{18} column (250 mm × 4.6 mm, 5 μm; Young Jin Biochrom Co., Ltd., Korea). A gradient elution of 0.5% acetic acid in water and methanol was used (0-30 minutes: 50% methanol, 30-45 minutes: 50% methanol, and 45-60 minutes: 50-10% methanol). The flowrate and injection volume were 1 mL/min and 10 μL, respectively. The UV detector was set at 270 nm.

Statistical analyses

All experiments were conducted in triplicate. Student's t-test and one-way analysis of variance were employed to evaluate the statistical significance among groups. Significant differences were expressed when the *P*-value was less than 0.05.

Results

EERH suppresses bladder cancer cell proliferation via the induction of G_1-phase cell cycle arrest

To investigate whether EERH inhibits T24 and 5637 bladder cancer cell proliferation, we used MTT assay and cell counting assay. Treatment of T24 cells with EERH significantly decreased the cell viability in dose-dependent manner (Figure 1A). In accordance with the result of cell viability, the number of T24 cells declined after treatment with EERH via utilization of Trypan Blue staining (Figure 1B). Similar results were observed in 5637 cells (Figure 1A and B). According to the proliferation assay, an IC_{50} value of EERH was determined to be 800 μg/mL at both cells (Figure 1A and B). In addition, to examine the role of EERH in cell cycle distribution, both cells were treated with EERH for 24 hours, and then fluorescence-activated cell sorting (FACS) analysis was performed. FACS analysis showed that EERH treatment resulted in the accumulation of T24 and 5637 cells at G_1-phase, with a concomitant decline in the proportion of G_2/M-phase (Figure 1C–F). These results
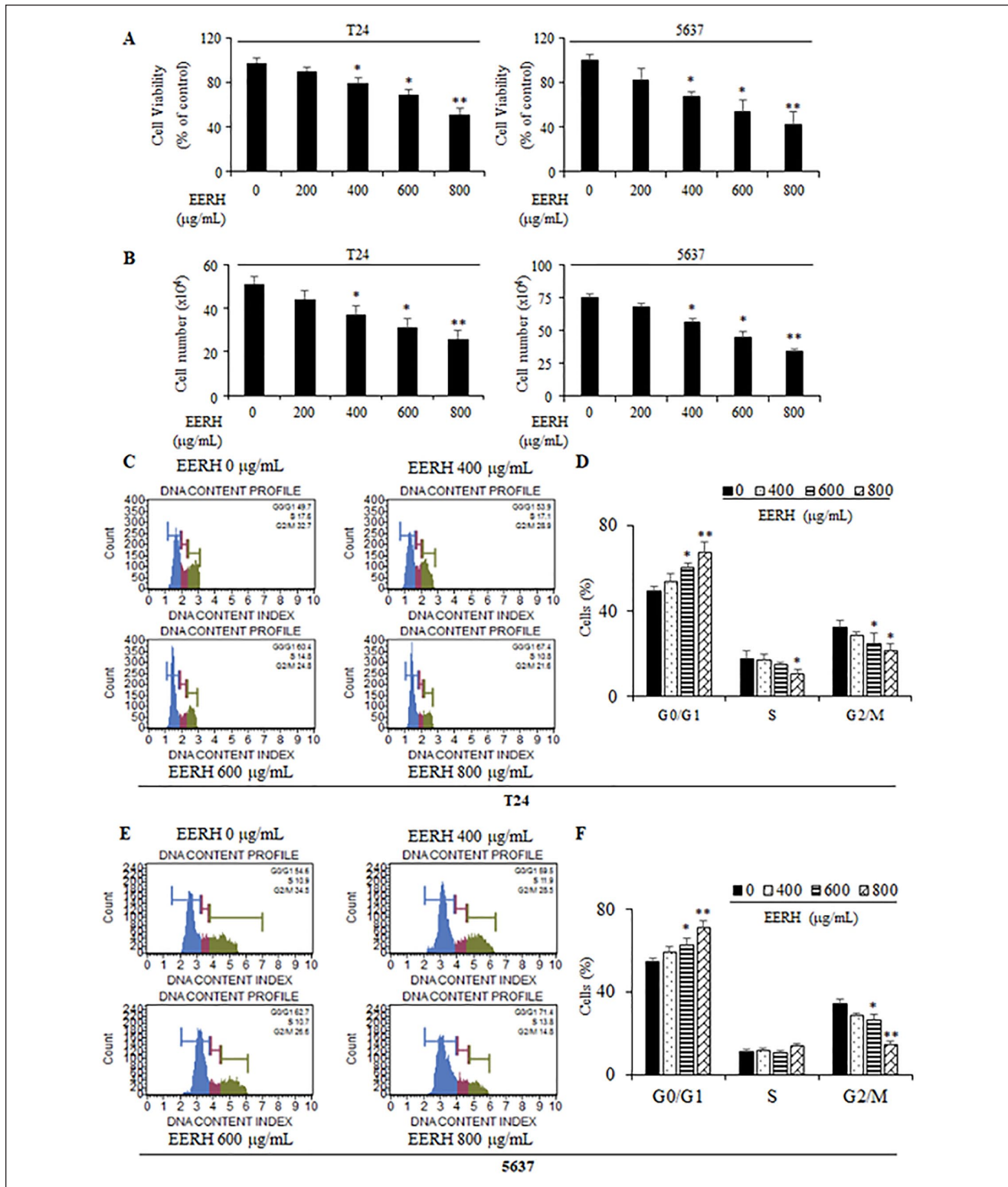
Figure 1. Effects of the EERH on cell proliferation and cell cycle in bladder cancer T24 and 5637 cells. T24 cells were incubated with various concentrations of EERH for 24 hours. (A) Viability of T24 and 5637 cells was measured using MTT assay. (B) The number of viable cells counted using a microscope. (C and E) Fluorescence-activated cell sorting (FACS) analysis of EERH-treated cells to determine the histogram of cell cycle pattern. (D and F) Percentages of cell population at each phase of cell cycle. The values are presented as the mean ± standard deviation (SD) of 3 independent experiments; *$P < .05$ and **$P < .01$ compared with the untreated control.

indicated that EERH inhibits bladder cancer cell proliferation through cell cycle arrest mainly occurring in the G_1-phase.

EERH-stimulated G_1-phase cell cycle arrest is implicated in the p21WAF1-mediated downregulation of the cyclins/CDKs complexes

Cyclins and CDKs are critical factors in the cell cycle progression from G_1- to S-phase.[6-8] To investigate the mechanism of G_1-phase cell cycle arrest in EERH-treated T24 cells, expression levels of cyclin D1, cyclin E, CDK2, and CDK4 were examined. Immunoblot results showed that cyclin D1 and CDK4 levels were decreased after treatment with EERH in T24 cells (Figure 2A). However, levels of cyclin E and CDK2 were not altered in the presence of EERH (Figure 2A). In addition, cyclin D1, cyclin E, CDK2, and CDK4 levels were declined in EERH-treated 5637 cells (Figure 2B). CDKIs mediate the control of cyclins/CDKs complexes during the G_1-phase cell cycle arrest.[6-8,10] Therefore, the protein levels of CDKIs, such as p21WAF1 and p27KIP1, were evaluated in T24 and 5637 cells using immunoblot. EERH treatment upregulated the expression levels of p21WAF1 in both cells (Figure 2A and B). In contrast, p27KIP1 levels were not changed by EERH treatment (Figure 2A and B). EERH treatment did not affect the expression levels of tumor suppressor protein p53 (Figure 2A and B). To define whether p21WAF1 expression contributes to the reduced expression of CDK2 and CDK4, immunoprecipitation (IP) assay was conducted. EERH-treated T24 cells were immunoprecipitated with antibodies against CDK4, then followed by immunoblot for p21WAF1 antibody. Exposure of T24 cells to EERH evidently enhanced the binding of p21WAF1 with CDK4 (Figure 2C). After IP with CDK2 and CDK4 antibodies in 5637 cells treated with EERH, immunoblot assay was performed with p21WAF1 antibody. EERH induced the p21WAF1 levels, which binds to CDK2 and CDK4 (Figure 2D). Similar results were observed in IP using p21WAF1 antibodies (Figure 2C and D). These results suggested that EERH-promoted G_1-phase cell cycle arrest was involved in the p21WAF1-mediated downregulation of cyclins/CDKs complexes.

MAPKs and AKT signaling is regulated during EERH-treated bladder cancer cell proliferation

We next examined the impact of EERH on the MAPKs (ERK1/2, p38MAPK, and JNK) and AKT signaling pathways in bladder cancer cells. EERH treatment showed increased phosphorylation of ERK1/2, p38MAPK, and JNK in T24 cells (Figure 3A). In addition, treatment of T24 cells with EERH also upregulated the phosphorylation of AKT

(Figure 3A). However, AKT phosphorylation was decreased and phosphorylation levels of ERK1/2, p38MAPK, and JNK were increased in EERH-treated 5637 cells (Figure 3B). To confirm the elevated levels of MAPKs and AKT phosphorylation in EERH-treated cells, their specific inhibitors were employed. Pretreatment of SB203580 (p38MAPK specific inhibitor) inhibited EERH-stimulated p38MAPK phosphorylation in both bladder cancer cell lines (Figure 3C and D). However, increased phosphorylation levels of ERK1/2 and JNK by EERH were not affected in the pretreatment of U0126 (ERK1/2 inhibitor) and SP600125 (JNK inhibitor) in T24 cells (Figure 3C), while EERH-induced phosphorylation levels of ERK1/2 and JNK were reduced in 5637 cells (Figure 3D). In addition, LY294002 (AKT inhibitor) inhibited AKT phosphorylation in EERH-treated T24 cells (Figure 3C). These results demonstrated that EERH differently regulates the phosphorylation of MAPKs and AKT signaling in bladder cancer cells.

Transcription factors-mediated MMP-9 expression is associated with EERH-stimulated suppression of bladder cancer cell migration and invasion

To estimate the metastatic potential of EERH in bladder cancer cells, we used the wound-healing assay and Boyden chamber assay in T24 and 5637 cells. Treatment of both cells with EERH induced inhibition of wound closure (Figure 4A). In accordance with the result from scratch assay, invasiveness of both cells was attenuated in the presence of EERH (Figure 4B). The number of invasive cells traversing transwell membrane was significantly alleviated after treatment with EERH (Figure 4B). Based on the zymographic and immunoblot assay, EERH treatment showed significant reduction in MMP-9 expression (Figure 4C and D). The expression levels of MMP-2 also decreased by treatment with EERH (Figure 4C and D). In order to determine the transcriptional regulation of MMP-9 in EERH-treated bladder cancer cells, EMSA experiment was performed. EERH treatment led to the obvious decline in binding ability of AP-1, NF-κB, and Sp-1 to MMP-9 promoter region (Figure 4E and F). These results revealed that EERH impedes the migration and invasion of bladder cancer cells via reduction of MMP-9 expression by impaired binding activity of transcription factors.

EERH mitigated tumor growth in the xenograft mice injected with T24 bladder cancer cells without apparent toxicity

To further assess the antitumor efficacy of EERH, xenograft mice bearing T24 bladder cancer were generated. Daily oral injection with 20 and 200 mg/kg of EERH for 20 days
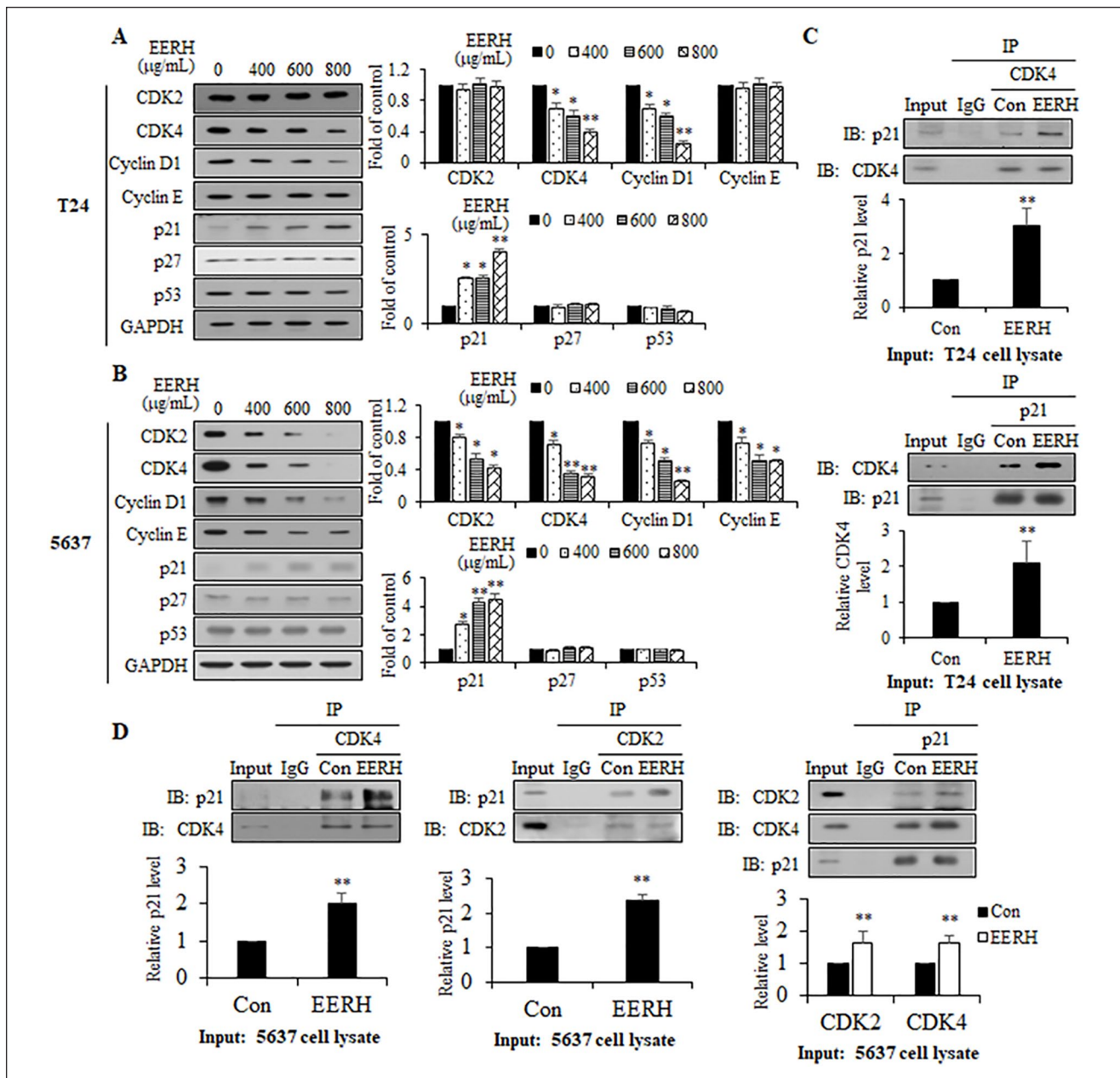
Figure 2. Effects of EERH on the cell cycle regulatory proteins. (A and B) Immunoblotting results for cyclin D1, cyclin E, cyclin-dependent kinase (CDK)−2, CDK4, p27KIP1, p21WAF1, and p53 for cells treated with indicated concentrations of EERH. Glyceraldehyde 3-phosphate dehydrogenase (GAPDH) was utilized as the internal control. (C and D) Cell lysates from T24 and 5637 cells treated with EERH for 24 hours were immunoprecipitated with antibodies against p21WAF1, CDK2, and CDK4 and then immunocomplexes were subjected to immunoblotting using cell lysates. Normal rabbit IgG and mouse control IgG were used as IgG control. The values are presented as the mean ±SD of 3 independent experiments; *$P < .05$ and **$P < .01$ compared with the untreated control.

revealed an evident reduction in tumor weight of xenograft mice (Figure 5A). The tumor volume of 20 mg/kg and 200 mg/kg EERH group was significantly decreased compared to the control group (Figure 5C). A decline in tumor weight and volume at 200 mg/kg EERH was comparable to that of 5 mg/kg cisplatin (Figure 5A and C). In addition,

H&E histological staining of the tumor tissues excised from EERH-treated mice resulted in a significantly decreased number of cancer cells in comparison to those of non-treated mice (vehicle) (Figure 5D). Moreover, EERH treatment did not result in significant body weight loss of the xenograft mice (Figure 5B). However, the mice administered with
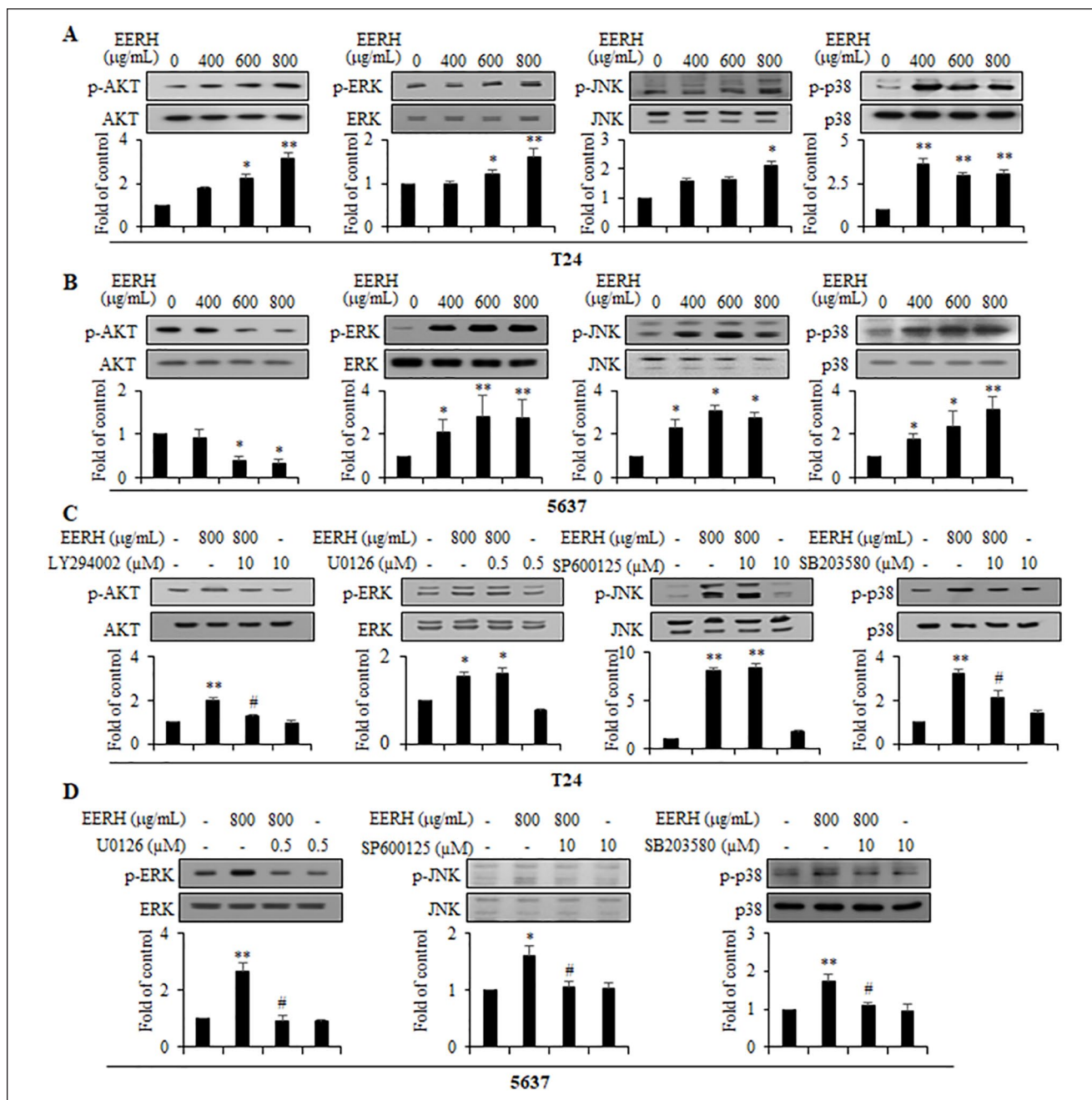
Figure 3. Effects of EERH on the cell signaling pathway. (A and B) Immunoblotting for total and phosphorylated forms of AKT, ERK1/2, JNK, and p38MAPK in cells incubated with EERH for 24 hours. (C and D) Cells were pre-incubated with signaling inhibitors of SB203580 (10 μM), U0126 (0.5 μM), LY 294002 (10 μM), and SP600125 (10 μM) for 40 minutes, followed by EERH treatment for 24 hours. Immunoblotting was performed using cell lysates. Total forms were utilized as internal control. The values are presented as the mean ±SD of 3 independent experiments; *$P < .05$ and **$P < .01$ compared with the untreated control.

cisplatin exhibited approximately 22% loss of body weight (Figure 5B). To further investigate the safety of EERH, single dose acute toxicity assay was performed. During oral administration of 2000 mg/kg EERH for 14 days, no toxic signs were observed in any mice, such as hematological analysis (AST, ALT, ALP, urea, and creatinine) and body weight loss (Figure 6A and B). Histological analysis displayed no pathological abnormality in organ tissues such as kidney, liver, and lung between treatment and no-treatment groups (Figure 6C). Angiogenic potential is a crucial step in the progression and development of tumors.[17,18,20] We next performed immunostaining experiment to detect
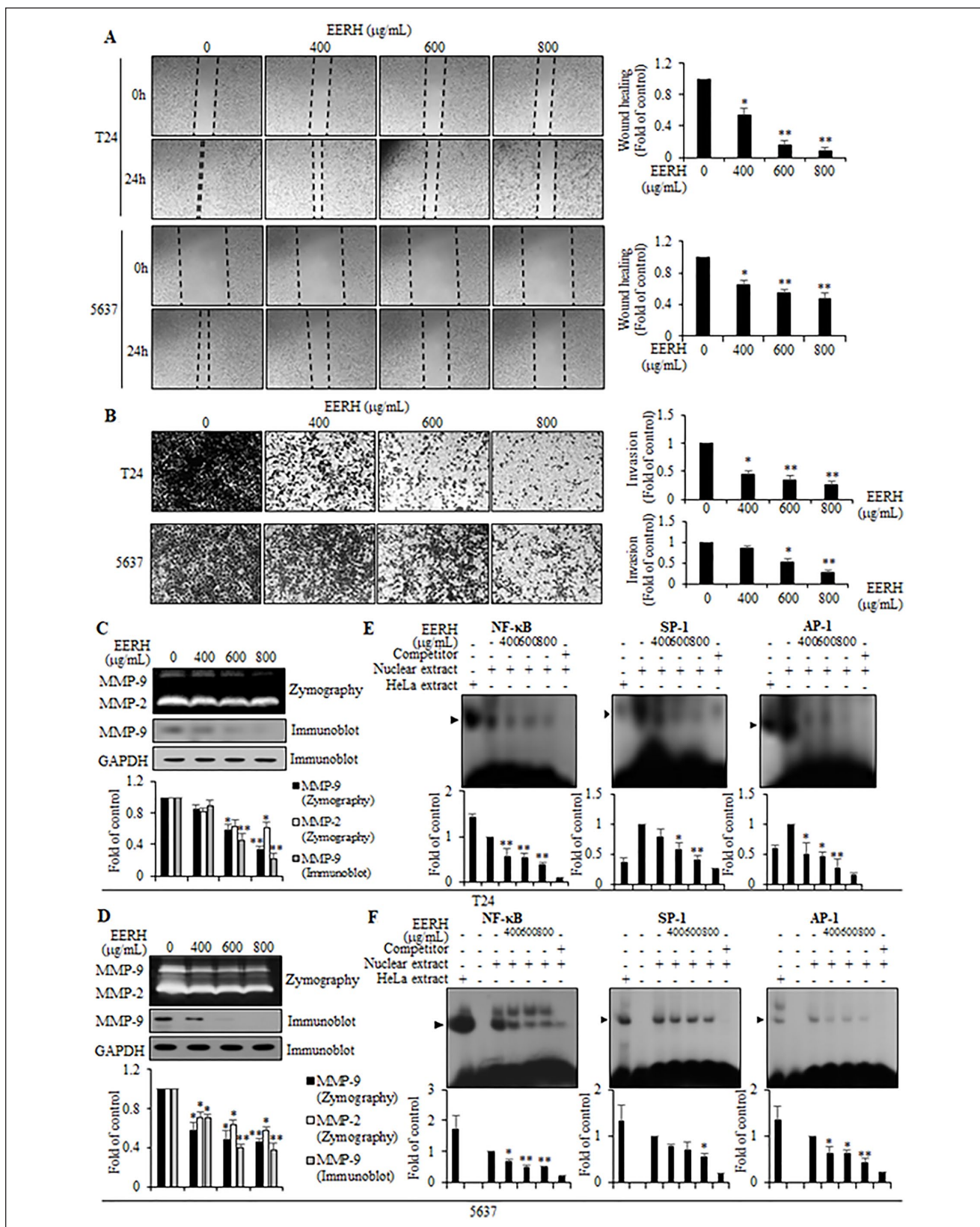
Figure 4. *(continued)*

Figure 4. Effects of EERH on the migration, invasion, and transcription factors-controlled matrix metalloproteinase (MMP)-9 expression in bladder cancer cells. Cells were treated with indicated concentrations of EERH. (A) The distance between wounded areas was photographed (40× magnification) and visualized by inverted microscope. (B) Cells that invaded the bottom side of the membrane were stained and counted. (C and D) Activity and expression of MMP-9 was analyzed using zymography and immunoblotting. GAPDH was utilized as internal control. (E and F) Transcriptional activation of Sp-1, AP-1, and NF-κB was determined by electrophoretic mobility shift assay (EMSA) with radiolabeled oligonucleotide probes. All data are expressed as the means ± standard error (SE) of 3 experiments. **$P < .05$ and **$P < .01$ compared with the untreated control.
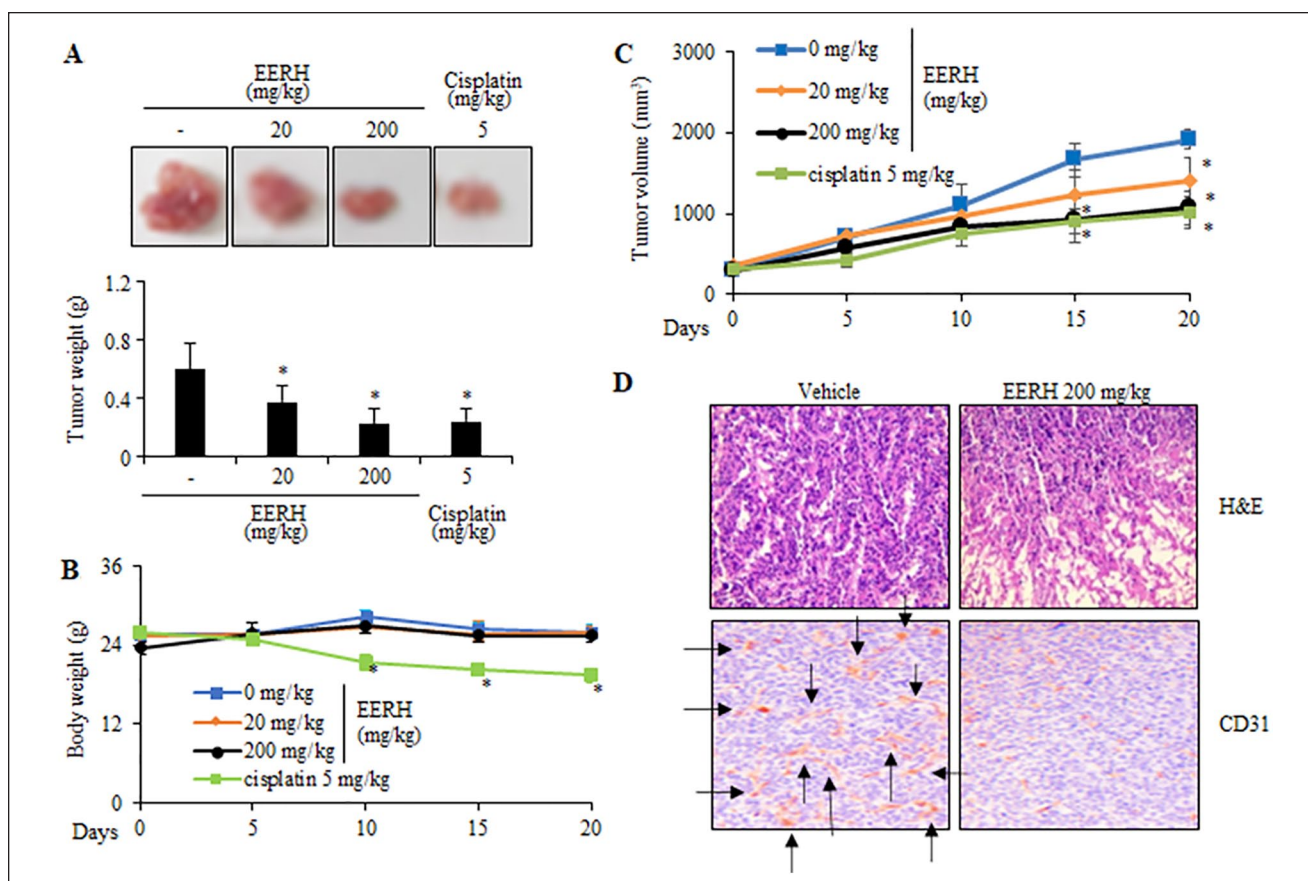

Figure 5. Anti-tumor efficacy of oral administration of EERH in the T24 bladder cancer xenograft mice. (A) Growth and weights of representative isolated tumors. (B) Body weights of mice with EERH treatment were compared with those of mice with cisplatin treatment. (C) Tumor volume was measured every 5 days. (D) Staining of growing tumor cells (H&E) and microvessel density (CD31) in tumor tissues. For (A-C), all data are expressed as the mean ± SE of 3 experiments. *$P < .05$ compared with the untreated control.

microvessel density in EERH-treated intratumor tissues using CD31 protein, which is an endothelial cell marker. The CD31 expression levels were markedly suppressed in the tumors from EERH-treated mice as compared with the non-treated mice tumors, which indicates that the antitumor effect of EERH is closely linked with angiogenic blood vessel regulators (Figure 5D).

EERH impeded VEGF-induced HUVEC proliferation by suppressing VEGFR2-mediated eNOS/AKT/ERK1/2 signaling axis

Upon identification of CD31 inhibition in EERH-treated tumor tissues, we examined whether EERH could affect the

angiogenic regulatory mechanism in HUVECs. Both MTT assay and cell counting assay were utilized to determine the effect of EERH on HUVEC proliferation in the absence or presence of VEGF (20 ng/mL). EERH alone at 10, 20, and 40 μg/mL exhibited no effect on the cell viability (Figure 7A). EERH treatment at 40 μg/mL reversed the VEGF-induced cell viability to the basal line (Figure 7A). Similar results were obtained in cell counting assay using trypan blue staining, which indicated that EERH impaired the VEGF-stimulated proliferation of HUVECs (Figure 7B). We next investigated the effect of EERH on the VEGFR2-mediated signaling network including eNOS/AKT/ERK1/2, which is involved in molecular action of angiogenesis in VEGF-treated HUVECs. VEGF treatment induced phosphorylation
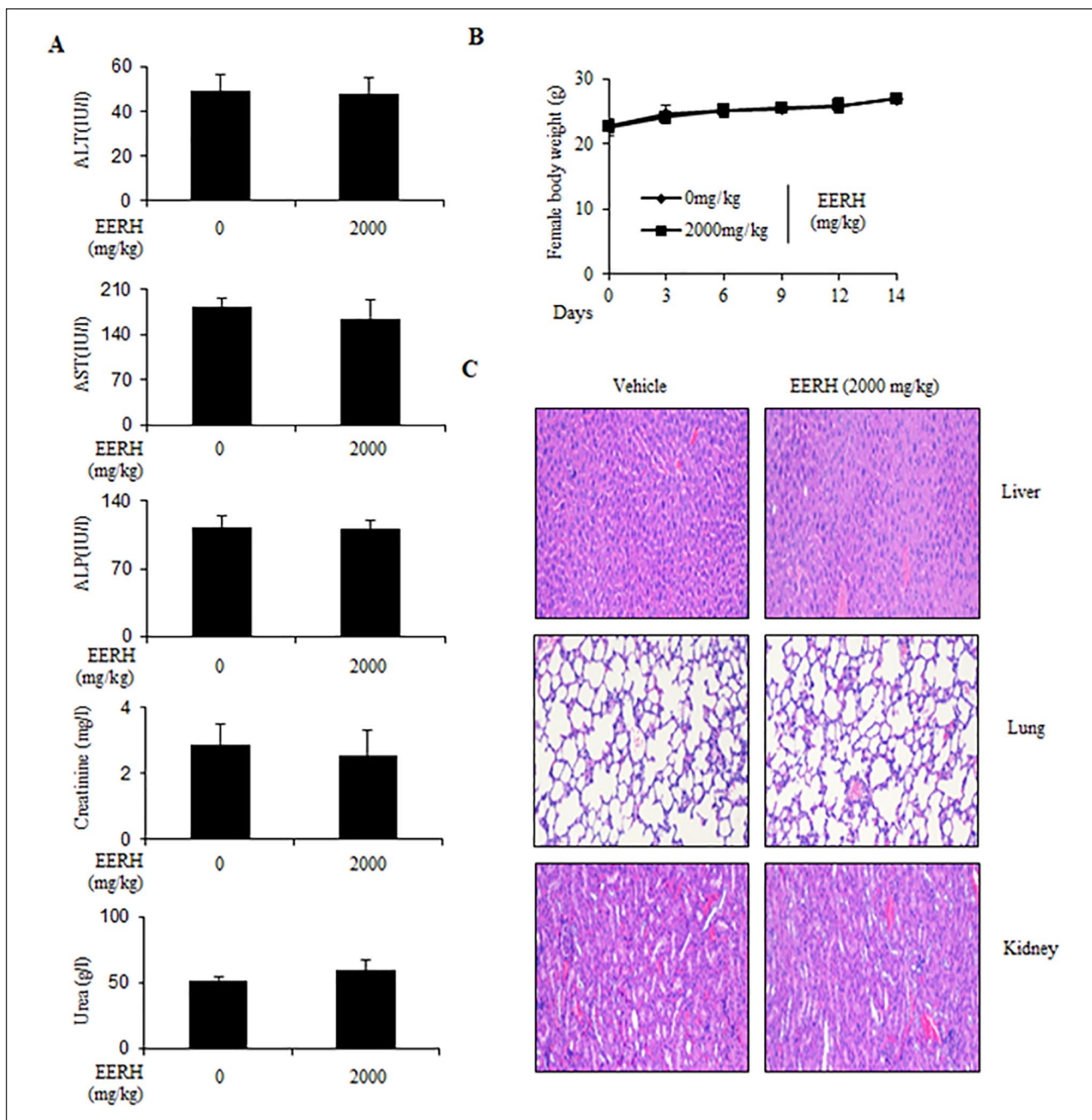
Figure 6. A single dose acute toxicity test of the mice administered with EERH on 14 days. Mice were orally administered with EERH (2000 mg/kg) for 14 days. (A) Analysis of biochemical test (AST, ALT, ALP, urea, and creatinine) between control and EERH-treated mice. (B) Changes in the body weights were observed in the EERH-treated mice. (C) H&E staining results of 3 main organs (kidney, liver, and lung) in mice orally injected EERH. For (A and B), values are presented as the mean ± SD of 3 independent experiments; *$P < .05$ compared with the control group.

of VEGFR2 (Figure 7F). VEGF-stimulated phosphorylation of VEGFR2 was interfered with in the presence of EERH (Figure 7F). In addition, phosphorylation of eNOS, AKT, and

ERK1/2 was stimulated by VEGF treatment, while the treatment with EERH led to a decrease in VEGF-induced phosphorylation of eNOS, AKT, and ERK1/2 (Figure 7C–E).
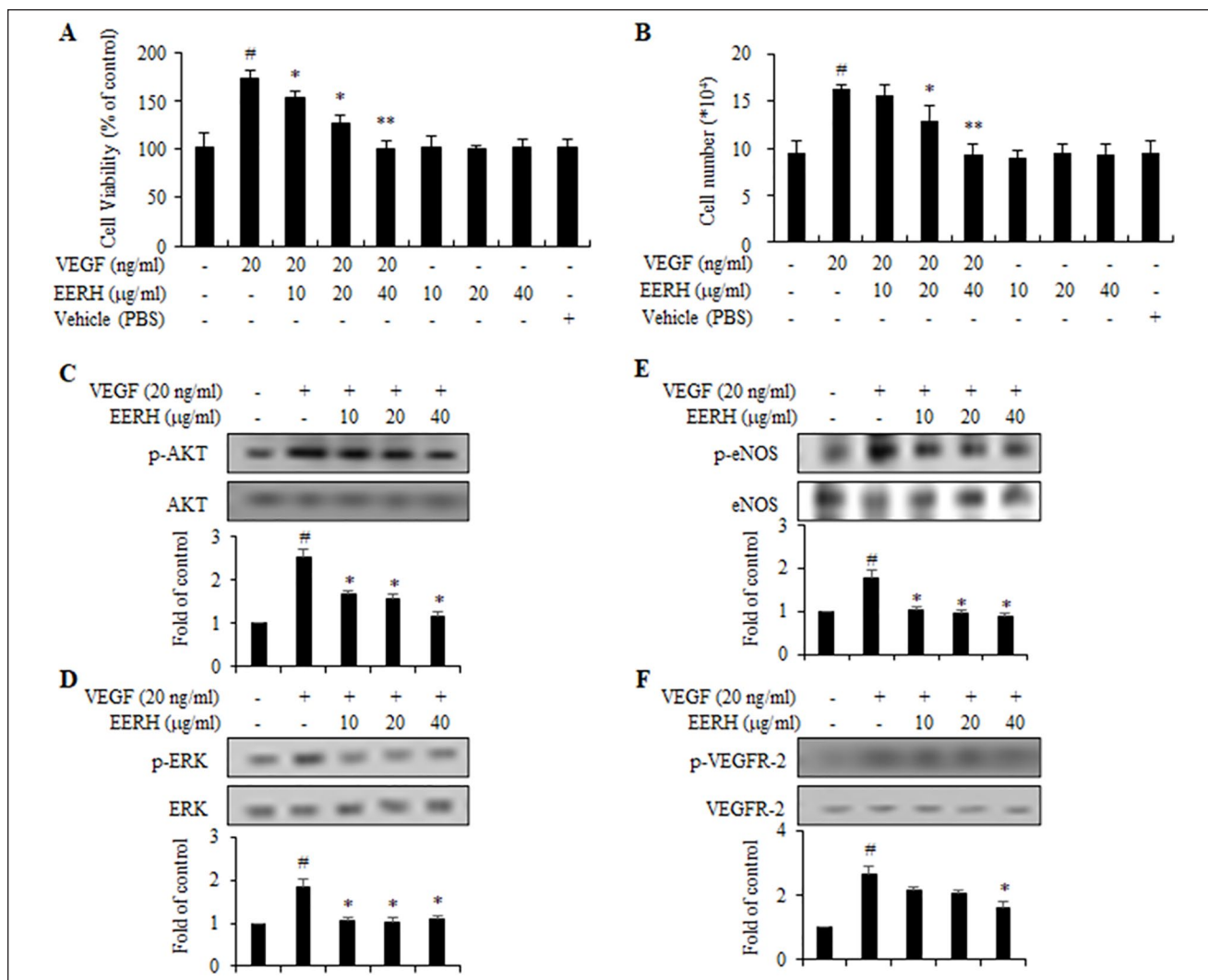
Figure 7. EERH impeded the proliferation and VEGFR2-driven eNOS/AKT/ERK1/2 signaling in the VEGF-stimulated HUVECs. Cells were incubated with indicated concentrations of EERH for 40 minutes, prior to treatment with VEGF (20 ng/mL) for 24 hours. Cell proliferation was determined by both cell viability assay (A) and cell counting assay (B). (C-F) Cell lysates were prepared and phosphorylated level of VEGFR2, eNOS, AKT, and ERK1/2 was evaluated by immunoblot experiment. All data are shown as the means ± SE of 3 experiments. #$P < .05$ compared with control. *$P < .05$ and **$P < .01$ compared with VEGF treatment.

Effects of EERH on colony tube formation, migration, invasion, and expression levels of MMP-2 in HUVECs induced by VEGF

We assessed whether EERH could inhibit the colony tube formation, migration, and invasion in VEGF-treated HUVECs. Treatment with VEGF allowed formation of the capillary-like tube on the Matrigel, whereas the building of colony tube structure in HUVECs co-cultured with VEGF and EERH was abrogated (Figure 8A). In addition, migratory and invasive efficacies of HUVEC cells were investigated by wound-healing and Matrigel invasion assays. VEGF treatment showed induction of wound closure rates in HUVECs, and treatment of cells with EERH resulted in the suppressed migratory ability (Figure 8B). Invasiveness of cells across pores was significantly increased in the treatment with VEGF, while EERH application prevented the invasive potency across the transwell plates in VEGF-treated HUVECs (Figure 8C). To further examine the role of EERH in VEGF-treated HUVECs, we determined the expression levels of MMP-2, which is a regulator closely associated with the migration and invasion of vascular cells.[28,29] MMP-2 level was evaluated by both zymography assay and immunoblot. Upon both assay systems, MMP-2 expression in HUVECs was rapidly increased in response to VEGF, meanwhile the utilization of EERH alleviated the VEGF-stimulated MMP-2 expression (Figure 8D).
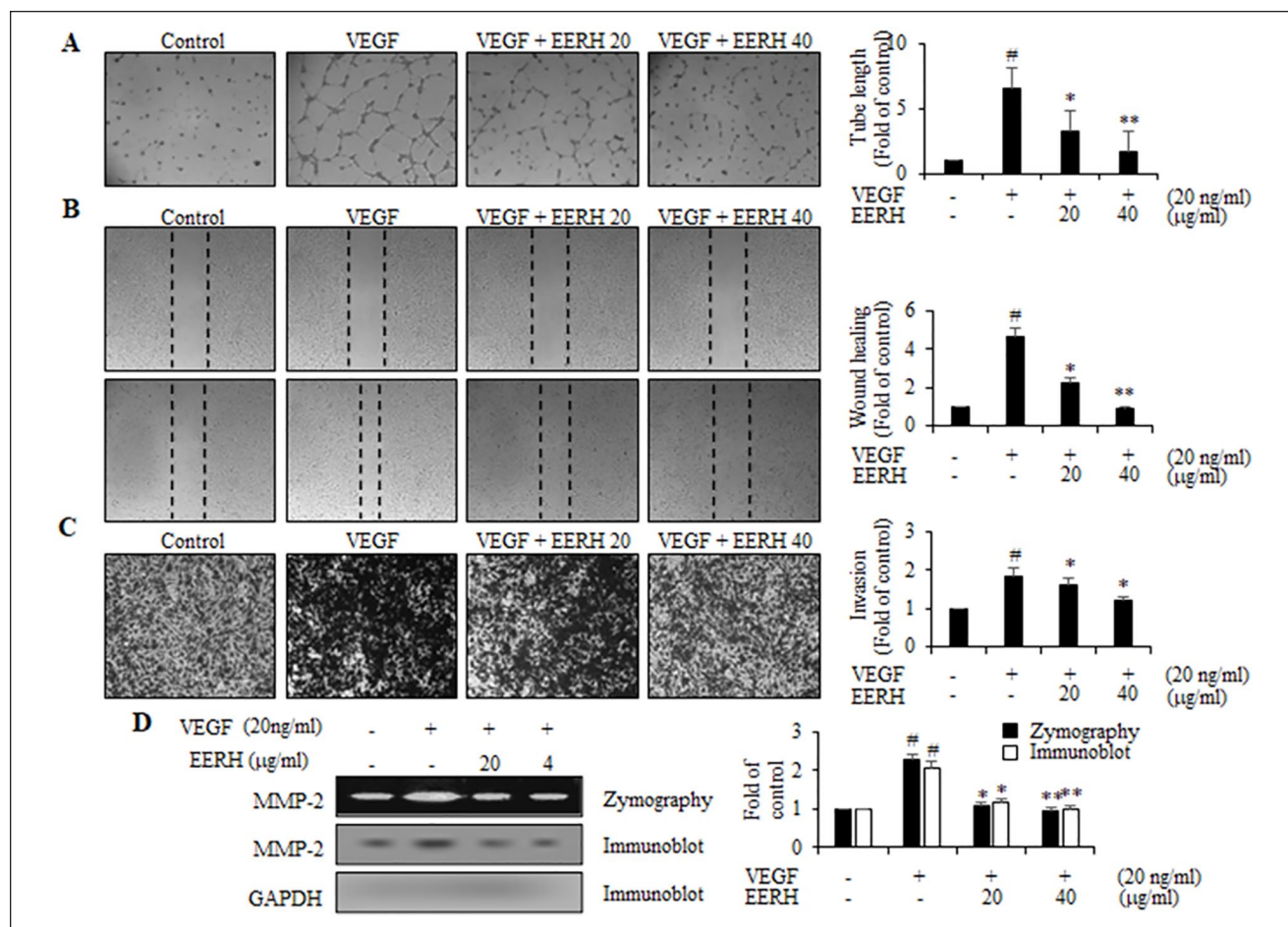
Figure 8. EERH suppressed the VEGF-stimulated angiogenic actions including colony tube formation, migration, invasion, and MMP-2 expression in HUVECs. After pre-treatment of cells with various concentrations of EERH for 40 minutes, cells were incubated with VEGF (20 ng/mL) for 24 hours. (A) The effect of EERH on colony tube formation assay using pre-coated Matrigel (scale bars = 200 μm). (B) Migratory potential of EERH was determined by wound-healing migration assay. (C) Transwell plate invasion assay was performed to examine the invasiveness of cells treated with EERH. (D) Gelatin zymographic assay and immunoblot experiment were employed to determine the activity and expression level of MMP-2. GAPDH was utilized as internal control. All data are obtained as the means ±SE of 3 experiments. #$P < .05$ compared with control. *$P < .05$ and **$P < .01$ compared with VEGF treatment.

EERH attenuated the VEGF-mediated angiogenic vessel formation in aortic ring sprouting ex vivo model

To evaluate the suppressive effect of EERH on VEGF-stimulated angiogenic responses, we performed an aortic ring assay ex vivo. Aortic fragments removed from mice were put on the Matrigel-coated plate pre-treated with VEGF. The formation of vessel sprouting around aortic area on the Matrigel was expanded with VEGF treatment (Figure 9). However, treatment with EERH markedly prevented the VEGF-stimulated promotion of microvessel formation.

Identification of kaempferol and HPLC analysis

The antitumor effects of EERH fractions were investigated using the MTT and cell counting assays. As shown in

Figure 10B to D fraction of EERH showed the best antitumor efficacy against bladder cancer T24 cells. The major compound of the d-fraction from EERH was identified as kaempferol via NMR and MS analysis[42] and confirmed with HPLC analysis (Figure 10A) and 1H-NMR of kaempferol (Figure 10D).

Discussion

EERH is widely available in cosmetics and functional foods worldwide. Given the expanding commercial benefits and industrial development of EERH in healthcare application, comprehensive utilization of EERH for the prevention and management of aggressive cancer must be investigated. In this study, we evaluated the antitumor efficacy of EERH in bladder cancer using both in vitro experiments and in vivo xenograft model. In addition, we performed a safety
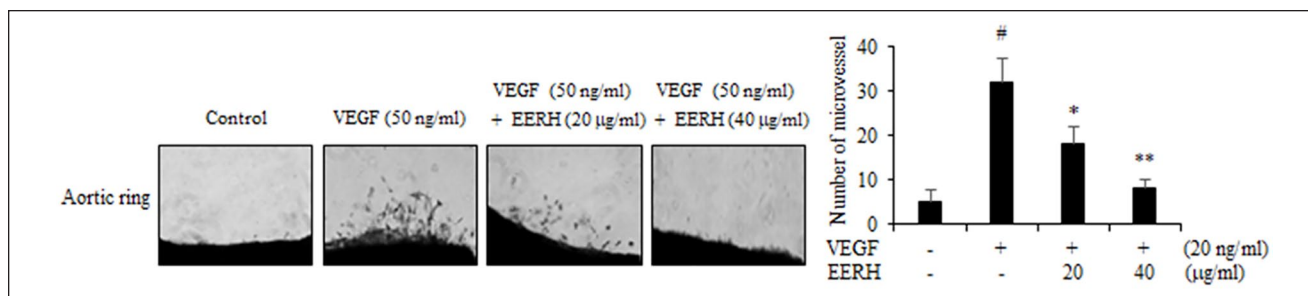
Figure 9. Effects of EERH on the VEGF-induced neovessel sproung using an aortic ring ex vivo model. Representative images of the microvascular sprouting formed in the aortic ring assay between EERH-treated group and control group. A number of neovessel sprouting emerging from aortic ring in each group was photographed and counted. All data are represented as the means ± SE of 3 experiments. $^{#}P < .05$ compared with control. $^{*}P < .05$ and $^{**}P < .01$ compared with VEGF treatment.

evaluation using the acute toxicity test. Moreover, the anti-angiogenic effect of EERH was established using an in vitro and ex vivo model. Furthermore, the main active compound of EERH was identified as kaempferol by spectroscopic analysis, HPLC analysis, and NMR analysis.

Promotion and development of bladder tumors depend on multiple functional processes that are involved in the uncontrolled proliferation and metastatic potential into surrounding extracellular matrix.[5-7] Therefore, primary targets of effective functional foods or natural molecules being developed for application against tumor treatment are the efficient inhibition of vigorous proliferation, rapid migration, and potent invasion derived from aggressive tumor cells.[5,7] In the first step of this study, we investigated the inhibitory effect of EERH on proliferation of T24 and 5637 cells. EERH treatment suppressed T24 and 5637 cell proliferation as demonstrated using the MTT and cell counting assays. To examine the regulatory mechanism in EERH-induced bladder cancer cell proliferation inhibition, both cell cycle and signaling pathways were employed. After the FACS analysis, immunoblotting, and IP, we determined that EERH-mediated cell proliferation retardation was because of the p21WAF1-associated dysregulation of cell cycle regulatory proteins, such as cyclin D1, cyclin E, CDK2, and CDK4, at the G_1-phase cell cycle arrest. After investigating the signaling pathways with immunoblotting, our data revealed that both the AKT and p38MAPK signaling were involved in EERH-stimulated T24 cells. EERH regulated the AKT, ERK1/2, JNK, and p38MAPK signaling in 5637 cells. These results indicated that EERH might inhibit the proliferation of bladder cancer cells via the p21WAF1-mediated G_1-phase cell cycle arrest and regulation of both AKT and MAPKs signaling pathways.

Another characteristic mechanism of cancer cells during bladder tumor promotion is migration and invasion of tumor cells by degrading the extracellular matrix.[11-14] In the present study, EERH treatment led to the reduction in migration and invasion of bladder cancer cells as determined by the wound-healing and transwell plate invasion assays. Previous studies have demonstrated the function of MMP-9 in tumor progression.[11-14] Overexpression of MMP-9 is remarkably associated with migration and invasion of bladder cancer cells in cell lines and clinical studies.[13,14] Upregulated level of MMP-9 expression was potently regulated in response to transcription factors, including Sp-1, NF-κB, and AP-1, in its promoter region.[6,7,15,16] The results showed that treatment with EERH suppressed expression of MMP-9 and binding ability of transcription factors Sp-1, NF-κB, and AP-1 to its proximal cis-element in the MMP-9 promoter. Earlier studies showed that the rose petal extract can suppress MMP-9 expression and migration and invasion of vascular smooth muscle cells (VSMC) and some cancer cells.[41,43,44] Similarly, it was demonstrated that the rose petal extract inhibited the binding activity of transcription factors in VSMCs.[41] However, the present study suggests the first regulatory mechanism demonstrating inhibition of migration and invasion of cancer cells induced by reduced transcription factor-mediated MMP-9 expression. Our findings strongly indicated that EERH treatment might be responsible for the strong anti-metastatic potential in bladder cancer. The role of MMP-2 regulation in EERH-treated cancer cells needs to be elucidated.

Besides the cellular study of EERH in vitro, antitumor efficacy of EERH was explored for the first time in xenograft mice transplanted with T24 cells. Administration of EERH could suppress the tumor growth in mice bearing the bladder cancer cells as demonstrated by measurement of the weight and volume of tumors and the execution of immunostaining. After 200 mg/kg EERH treatment, reduction of tumor weight and volume was comparable to the treatment with 5 mg/kg cisplatin, which demonstrated adverse effects. In an acute toxicity test, application of 2000 mg/kg EERH revealed no toxic signs using biochemical analysis and H&E staining. These results demonstrated that EERH administration exhibited potent antitumor efficiency to hinder tumor growth, which is not ascribed to its toxicity. The
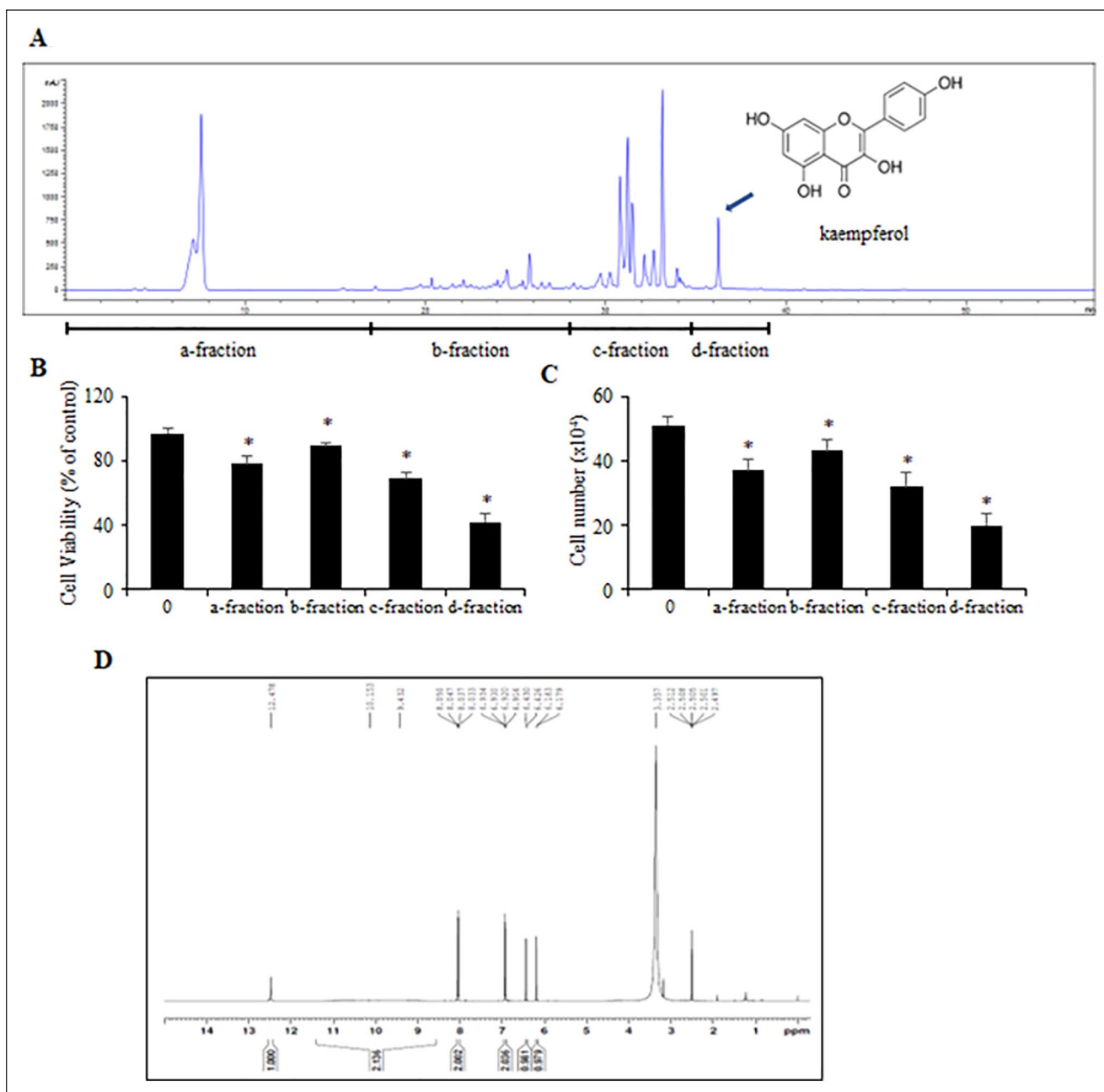
Figure 10. (A) HPLC chromatogram of EERH and chemical structure of active compound kaempferol. (B and C) MTT assay and cell counting analysis was employed to determine the anti-tumor effect in the sub-fractions of the EtOAc fraction from EERH.
(D) ^{1}H-NMR of kaempferol. The values are presented as the mean ± SD of 3 independent experiments; *$P < .05$ compared with the untreated control.

present results suggested that EERH could be utilized as an effective and safe natural supplement or drug for prevention and treatment of bladder cancer.

Some studies have addressed the role and function of angiogenesis during formation, progression, and development of tumors.[17,18] Our data demonstrated that the decreased expression of angiogenic endothelial marker CD31 was

detected in EERH-treated tumor tissues using immunostaining experiment. Therefore, we postulated that application of EERH could be a novel candidate for cancer prevention and treatment. In the present study, EERH inhibited the VEGF-induced proliferation in HUVECs. Activation of VEGFR2-driven eNOS/AKT/ ERK1/2 signaling was also attenuated in VEGF-treated HUVECs. Moreover, treatment of

HUVECs with EERH weakened the VEGF-mediated angiogenic potential of HUVECs by modulating their tube formation, migration, invasion, and expression of MMP-2. Finally, VEGF-stimulated neovessel sprouting from the aortic rings was attenuated by treatment with EERH. During progression and development of tumor formation, cancer cells require the microenvironment followed by enough supply of nutrients and oxygen to the tumor cells.[45,46] Blockade of neovessel formation prevents the sufficient supply of oxygen and nutrients into the tumor mass, and the inability of cancer cells to progress to the appropriate size led to the failure of tumor formation.[47,48] Previous studies have demonstrated that anti-angiogenic molecules can enhance the therapeutic effects of any anticancer drugs.[49,50] Here, we suggest that EERH can be a used for the development of an effective anticancer drug against bladder cancer by inhibiting tumor angiogenesis.

Studies have demonstrated that the rose petal extract contains several types of flavonoids, such as quercetin, pelargonidin, cyanidine, and kaempferol glycosides.[51,52] Result from our previous study showed that kaempferol isolated from rose petal exhibited aldose reductase inhibitory activity.[35] Based on the result from MTT and cell counting assays, demonstrating inhibition of T24 cell proliferation by EERH fractions, quality standardization of EERH was performed. The main active component of EERH was identified as kaempferol, which is involved in its antitumor activity. Importantly, kaempferol has long attracted much attention owing to its several biological functions, including anticancer effects.[53] In the present study, HPLC analysis of the EERH revealed the presence of kaempferol. Thus, we report that kaempferol is the main active compound of EERH, which is responsible for its antitumor efficacy. However, further studies are needed to isolate kaempferol from EERH and to identify its efficacy using in vitro cell lines and animal models.

Conclusion

In the present study, we revealed the therapeutic potential of EERH via the suppression of tumor growth and angiogenesis and highlighted anti-angiogenic and anti-tumorigenic activities of EERH against bladder cancer without any toxicity using mice models. EERH exerted in vitro and in vivo antitumor efficacy associated with cell cycle regulation, signaling pathway, and transcription factor-mediated metastatic suppression. Treatment with EERH exhibited anti-angiogenic activity in vitro, involving colony tube formation, proliferation, migration, and invasion of HUVECs via the VEGFR-2-modulated eNOS/AKT/ERK1/2 signaling cascade and MMP-2 expression. EERH was able to inhibit the formation of neovessel using the aortic ring ex vivo assay. EERH did not show any adverse effects as evidenced by the acute toxicity test. Based on the chemical analysis, kaempferol was found to be the main active compound responsible for the antitumor effects of EERH. As a further study, to identify other signaling pathways involved in EERH-mediated antitumor effects and angiogenesis inhibition effects, gene expression analysis such as PCR array, microarray, and next-generation sequencing will be required. Finally, we suggest that EERH may be a potential candidate in future clinical trial as an antitumor agent for the treatment of bladder cancer.

Author Contributions

Conceptualization: Byungdoo Hwang and Sung-Kwon Moon; Data curation: Byungdoo Hwang, Yujeong Gho, Hoon Kim, Soon Auck Hong, and Tae Jin Lee; Investigation: Byungdoo Hwang, Yujeong Gho, Hoon Kim, and Soon Auck Hong; Project administration: Sung-Kwon Moon; Validation: Hoon Kim and Soon Auck Hong; Writing—original draft: Byungdoo Hwang and Sung-Kwon Moon; Writing—review and editing: Sanghyun Lee, Tae Jin Lee, Soon Chul Myung, Seok-Joong Yun, Yung Hyun Choi, Wun-Jae Kim, and Sung-Kwon Moon; Final approval of manuscript: All authors.

ORCID iD

Sung-Kwon Moon 🆔 https://orcid.org/0000-0002-4514-3457

References

1. Bray F, Ferlay J, Soerjomataram I, Siegel RL, Torre LA, Jemal A. Global cancer statistics 2018: GLOBOCAN estimates of incidence and mortality worldwide for 36 cancers in 185 countries. *CA Cancer J Clin*. 2018;68:394-424.
2. Kamat AM, Hahn NM, Efstathiou JA, et al. Bladder cancer. *Lancet*. 2016;388:2796-2810.
3. Smith AB, Deal AM, Woods ME, et al. Muscle-invasive bladder cancer: evaluating treatment and survival in the National Cancer Data Base. *BJU Int*. 2014;114:719-726.

4. Schneider AK, Chevalier MF, Derré L. The multifaceted immune regulation of bladder cancer. *Nat Rev Urol*. 2019; 16:613-630.

5. Black PC, Dinney CP. Bladder cancer angiogenesis and metastasis--translation from murine model to clinical trial. *Cancer Metastasis Rev*. 2007;26:623-634.

6. Lee SJ, Cho SC, Lee EJ, et al. Interleukin-20 promotes migration of bladder cancer cells through extracellular signal-regulated kinase (ERK)-mediated MMP-9 protein expression leading to nuclear factor (NF-κB) activation by inducing the up-regulation of p21(WAF1) protein expression. *J Biol Chem*. 2013;288:5539-5552.

7. Song JH, Park J, Park SL, et al. A novel cyclic pentadepsipeptide, N-methylsansalvamide, suppresses angiogenic responses and exhibits antitumor efficacy against bladder cancer. *Cancers*. 2021;13:191.

8. Prasad SB, Yadav SS, Das M, et al. PI3K/AKT pathway-mediated regulation of p27(Kip1) is associated with cell cycle arrest and apoptosis in cervical cancer. *Cell Oncol*. 2015;38:215-225.

9. Qi YL, Li Y, Man XX, et al. CXCL3 overexpression promotes the tumorigenic potential of uterine cervical cancer cells via the MAPK/ERK pathway. *J Cell Physiol*. 2020;235: 4756-4765.

10. Otto T, Sicinski P. Cell cycle proteins as promising targets in cancer therapy. *Nat Rev Cancer*. 2017;17:93-115.

11. Robertson AG, Kim J, Al-Ahmadie H, et al. Comprehensive molecular characterization of muscle-Invasive bladder cancer. *Cell*. 2017;171:540-556.e25.

12. Knowles MA, Hurst CD. Molecular biology of bladder cancer: new insights into pathogenesis and clinical diversity. *Nat Rev Cancer*. 2015;15:25-41.

13. Bianco F, Gervasi DC, Tiguert R, et al. Matrix metalloproteinase-9 expression in bladder washes from bladder cancer patients predicts pathological stage and grade. *Clin Cancer Res*. 1998;4:3011-3016.

14. Davies B, Waxman J, Wasan H, et al. Levels of matrix metalloproteases in bladder cancer correlate with tumor grade and invasion. *Cancer Res*. 1993;53:5365-5369.

15. Bond M, Fabunmi RP, Baker AH, Newby AC. Synergistic upregulation of metalloproteinase-9 by growth factors and inflammatory cytokines: an absolute requirement for transcription factor NF-kappa B. *FEBS Lett*. 1998;435:29-34.

16. Sato H, Seiki M. Regulatory mechanism of 92 kDa type IV collagenase gene expression which is associated with invasiveness of tumor cells. *Oncogene*. 1993;8:395-405.

17. Folkman J, Shing Y. Angiogenesis. *J Biol Chem*. 1992;267: 10931-10934.

18. Carmeliet P. Angiogenesis in life, disease and medicine. *Nature*. 2005;438:932-936.

19. Risau W. Mechanisms of angiogenesis. *Nature*. 1997;386: 671-674.

20. Tarallo V, De Falco S. The vascular endothelial growth factors and receptors family: up to now the only target for anti-angiogenesis therapy. *Int J Biochem Cell Biol*. 2015; 64:185-189.

21. Chung AS, Ferrara N. Developmental and pathological angiogenesis. *Annu Rev Cell Dev Biol*. 2011;27:563-584.

22. Shibuya M. Role of VEGF-flt receptor system in normal and tumor angiogenesis. *Adv Cancer Res*. 1995;67:281-316.

23. Fong GH, Rossant J, Gertsenstein M, Breitman ML. Role of the Flt-1 receptor tyrosine kinase in regulating the assembly of vascular endothelium. *Nature*. 1995;376:66-70.

24. Seetharam L, Gotoh N, Maru Y, Neufeld G, Yamaguchi S, Shibuya M. A unique signal transduction from FLT tyrosine kinase, a receptor for vascular endothelial growth factor VEGF. *Oncogene*. 1995;10:135-147.

25. Gerber HP, McMurtrey A, Kowalski J, et al. Vascular endothelial growth factor regulates endothelial cell survival through the phosphatidylinositol 3'-kinase/Akt signal transduction pathway. Requirement for Flk-1/KDR activation. *J Biol Chem*. 1998;273:30336-30343.

26. Pedram A, Razandi M, Levin ER. Extracellular signal-regulated protein kinase/Jun kinase cross-talk underlies vascular endothelial cell growth factor-induced endothelial cell proliferation. *J Biol Chem*. 1998;273:26722-26728.

27. Dimmeler S, Fleming I, Fisslthaler B, Hermann C, Busse R, Zeiher AM. Activation of nitric oxide synthase in endothelial cells by Akt-dependent phosphorylation. *Nature*. 1999;399: 601-605.

28. Lamy S, Ruiz MT, Wisniewski J, et al. A prostate secretory protein94-derived synthetic peptide PCK3145 inhibits VEGF signalling in endothelial cells: implication in tumor angiogenesis. *Int J Cancer*. 2006;118:2350-2358.

29. Lamalice L, Le Boeuf F, Huot J. Endothelial cell migration during angiogenesis. *Circ Res*. 2007;100:782-794.

30. Yu K, Liu M, Dai H, Huang X. Targeted drug delivery systems for bladder cancer therapy. *J Drug Deliv Sci Tech*. 2020;56:101535.

31. Liu HS, Ke CS, Cheng HC, Huang CYF, Su CL. Curcumin-induced mitotic spindle defect and cell cycle arrest in human bladder cancer cells occurs partly through inhibition of aurora A. *Mol Pharmacol*. 2011;80:638-646.

32. Kamat AM, Sethi G, Aggarwal BB. Curcumin potentiates the apoptotic effects of chemotherapeutic agents and cytokines through down-regulation of nuclear factor-kappaB and nuclear factor-kappaB-regulated gene products in IFN-alpha-sensitive and IFN-alpha-resistant human bladder cancer cells. *Mol Cancer Ther*. 2007;6:1022-1030.

33. Arbiser JL, Klauber N, Rohan R, et al. Curcumin is an in vivo inhibitor of angiogenesis. *Mol Med*. 1998;4:376-383.

34. Bai Y, Mao QQ, Qin J, et al. Resveratrol induces apoptosis and cell cycle arrest of human T24 bladder cancer cells in vitro and inhibits tumor growth in vivo. *Cancer Sci*. 2010;101: 488-493.

35. Sun H, Zhang Z, Zhang T, et al. Resveratrol reverses cigarette smoke-induced urocystic epithelial-mesenchymal transition via suppression of STAT3 phosphorylation in SV-HUC-1-immortalized human urothelial cells. *Onco Targets Ther*. 2019;12:10227-10237.

36. Wigner P, Bijak M, Saluk-Bijak J. The Green anti-cancer weapon. The role of natural compounds in bladder cancer treatment. *Int J Mol Sci*. 2021;22:7787.

37. Fernandes L, Casal S, Pereira JA, Saraiva JA, Ramalhosa E. Edible flowers: a review of the nutritional, antioxidant, antimicrobial properties and effects on human health. *J Food Compos Anal*. 2017;60:38-50.

38. Yon JM, Kim YB, Park D. The ethanol fraction of white rose petal extract abrogates excitotoxicity-induced neuronal damage *in vivo* and *in vitro* through inhibition of oxidative stress and proinflammation. *Nutrients*. 2018;10:1375.

39. Jeon JH, Kwon SC, Park D, et al. Anti-allergic effects of white rose petal extract and anti-atopic properties of its hexane fraction. *Arch Pharm Res*. 2009;32:823-830.

40. Yang G, Park D, Lee SH, et al. Neuroprotective effects of a butanol fraction of *Rosa hybrida* petals in a middle cerebral artery occlusion model. *Biomol Ther*. 2013;21:454-461.

41. Lee SJ, Won SY, Park SL, et al. *Rosa hybrida* extract suppresses vascular smooth muscle cell responses by the targeting of signaling pathways, cell cycle regulation and matrix metalloproteinase-9 expression. *Int J Mol Med*. 2016;37: 1119-1126.

42. Quilantang NG, Limbo CA, Lee JS, Jacinto SD, Moon SK, Lee S. Aldose reductase inhibition of *Rosa hybrida* petals and its active component, kaempferol. *Hortic Environ Biotechnol*. 2020;61:601-607.

43. Rivas-García L, Quiles JL, Roma-Rodrigues C, et al. Rosa x hybrida extracts with dual actions: antiproliferative effects against tumour cells and inhibitor of Alzheimer disease. *Food Chem Toxicol*. 2021;149:112018.

44. Lim WC, Choi HK, Kim KT, Lim TG. Rose (Rosa gallica) petal extract suppress proliferation, migration, and invasion of human lung adenocarcinoma A549 cells through via the EGFR signaling pathway. *Molecules*. 2020;25:5119.

45. Verheul HM, Voest EE, Schlingemann RO. Are tumours angiogenesis-dependent? *J Pathol*. 2004;202:5-13.

46. Folkman J. Tumor angiogenesis: therapeutic implications. *New Engl J Med*. 1971;285:1182-1186.

47. Bagherpoorfard M, Soheili AR. A moving mesh method for mathematical model of capillary formation in tumor angiogenesis. *Iran J Sci Technol*. 2019;43:1745-1753.

48. Matsuoka A, Mizumoto Y, Ono M, et al. Novel strategy of ovarian cancer implantation: pre-invasive growth of fibrin-anchored cells with neovascularization. *Cancer Sci*. 2019; 110:2658-2666.

49. Liu W, Zhang J, Yao X, et al. Bevacizumab-enhanced anti-tumor effect of 5-fluorouracil via upregulation of thymidine phosphorylase through vascular endothelial growth factor A/vascular endothelial growth factor receptor 2-specificity protein 1 pathway. *Cancer Sci*. 2018;109:3294-3304.

50. Iwai T, Sugimoto M, Harada S, Yorozu K, Kurasawa M, Yamamoto K. Continuous administration of bevacizumab plus capecitabine, even after acquired resistance to bevacizumab, restored anti-angiogenic and antitumor effect in a human colorectal cancer xenograft model. *Oncol Rep*. 2016;36: 626-632.

51. Biolley JP, Jay M. Anthocyanins in modern roses: chemical and colorimetric features in relation to the colour range. *J Exp Bot*. 1993;44:1725-1734.

52. Biolley JP, Jay M, Viricel MR. Flavonoid diversity and metabolism in 100 Rosa X hybrida cultivars. *Phytochemistry*. 1994;35:413-419.

53. Kashyap D, Sharma A, Tuli HS, Sak K, Punia S, Mukherjee TK. Kaempferol -a dietary anticancer molecule with multiple mechanisms of action: recent trends and advancements. *J Funct Foods*. 2017;30:203-219.